Pharmaceutical Research, Vol. 26, No. 8, August 2009 (© 2009)
DOI: 10.1007/s11095-009-9908-0

Research Paper

Chitosan/TPP and Chitosan/TPP-hyaluronic Acid Nanoparticles: Systematic Optimisation of the Preparative Process and Preliminary Biological Evaluation

Alessandro Nasti,[1,2] Noha M. Zaki,[1,3] Piero de Leonardis,[1] Suwipa Ungphaiboon,[1] Proramate Sansongsak,[1] Maria Grazia Rimoli,[2] and Nicola Tirelli[1,4]

Received March 16, 2009; accepted May 7, 2009; published online June 9, 2009

Purpose. Chitosan is one of the most sought-after components for designing nanoparticles for drug delivery applications. However, despite the large number of studies, reproducibility is often an issue; generally more attention should be focused on purity and precise characterization of the starting material, as well as on the development of robust preparative procedures.
Methods. Using a rational experimental design, we have studied the influence of a number of orthogonal factors (pH, concentrations, ratios of components, different methods of mixing) in the preparation of chitosan/triphosphate (TPP) nanoparticles and in their coating with hyaluronic acid (HA), aiming at the minimisation of size polydispersity, the maximisation of zeta potential and long-term stability, and at the control over average nanoparticle size.
Results and conclusion. Three optimised nanoparticles have been developed (two uncoated and one HA-coated) and their toxicity on fibroblasts and macrophages has been evaluated: experiments showed the beneficial character of HA-coating in the reduction of toxicity (IC50 raised from 0.7–0.8 mg/mL to 1.8 mg/mL) and suggested that the uncoated chitosan/TPP nanoparticles had toxic effects following internalisation rather than membrane disruption.

KEY WORDS: chitosan; hyaluronic acid; macrophages; nanoparticles; toxicity.

INTRODUCTION

Our group is particularly interested in the design of nano-carriers for payloads delivered in a biological environment and, specifically, of nanoparticles responsive to physico-chemical or biological stimuli that characterise the target environment (1). For example, nanoparticles that undergo morphological transitions that modify release kinetics or uptake by cells in response to the presence of oxidants (2). It is not our aim to discuss here the biomedical applications of nano-carriers, which are thoroughly reviewed elsewhere (3–10). On the other hand, we want to specifically focus on a few issues important in the nanoparticle design.

a) a colloidal carrier is generally internalized through endocytosis, ending up in endosomes that with time produce an increasingly aggressive environment. In most cases, it is desired that the carrier escapes from these compartments, delivering a payload in the cytoplasm; the most common strategy to do so exploits the acidification of endosomal compartments, to either increase the local osmotic pressure up to the collapse of the endosomal membrane ("proton sponge" effect due to the protonation of amine groups (11,12), or produce hydrophobic and membrane-disrupting compounds (13,14).
b) in the absence of a specific target, the surface composition should allow a prolonged circulation in the body fluid of choice, i.e. it should be "stealth" enough to allow the diffusion of the nanoparticles throughout the site. Among the polymer structures that could be used for providing this protein-repellent character, besides the ubiquitous poly(ethylene glycol) (PEG), one could mention dextrans (15), poly(N-vinyl pyrrolidone) (16), poly(glycerol methacrylate) (17) and glycosoaminoglycans, such as heparin (15) or hyaluronic acid (HA) (18).
c) at the end of its life cycle, a carrier should be degraded to excretable or metabolisable products, showing negligible cytotoxicity throughout the life cycle. It is noteworthy that in this process the interactions between cells and nanoparticles are mostly dependent on the nanoparticle surface composition, and specifically on charge, but also on their size (19–21).

In order to prepare nanoparticles capable of endosomal escape through the proton-sponge effect, prolonged circula-

Electronic supplementary material The online version of this article (doi:10.1007/s11095-009-9908-0) contains supplementary material, which is available to authorized users.

Alessandro Nasti and Noha M. Zaki have equally contributed to this manuscript.

[1] School of Pharmacy, University of Manchester, Stopford Building, Oxford Road, Manchester, M13 9PT, UK.
[2] Department of Pharmaceutical Chemistry and Toxicology, University of Naples "Federico II", Via D. Montesano 49, 80131 Napoli, Italy.
[3] Department of Pharmaceutics, Faculty of Pharmacy, Ain Shams University, Monazamet El Wehda El Afrikia St., El Abbassia, Cairo, Egypt.
[4] To whom correspondence should be addressed. (e-mail: Nicola.tirelli@manchester.ac.uk)

tion and degradability, we have here focused our attention on chitosan-based nanoparticles displaying hyaluronic acid on the surface.

Chitosan is a versatile biomaterial derived from chitin (essentially poly(β-1,4-N-acetyl-D-glucose-2-amine)), which is one of the most abundant natural polysaccharides, found in the cell walls of microorganisms such as yeasts or other fungi, in the exoskeletons of crustaceans and insects and in several other specialized organs, such as the beaks of cephalopods. The products of chitin deacetylation are known under the generic name of "chitosan"; however, since this process can deliver polymers with markedly different properties, it is essential to characterise chitosan samples at least in terms of average MW and degree of deacetylation, in order to ensure reproducibility in the experimental results. A few mammalian enzymes, such as α-amylase or lysozyme can degrade chitosan, therefore it can be generally regarded as degradable (22). Chitosan has been extensively employed in the development of micro- or nano-carriers (23), with a specific focus on the use of complex actives such as nucleic acids, e.g. siRNA (24), or proteins (25), possibly having enzymatic activity (26). It is noteworthy that the activity of these nano-carrier systems towards a biological target may be affected by chitosan own biological properties, for example its anticancer activity (27).

Hyaluronic acid (HA), on the other hand, is one of the most sought after materials when degradability and biocompatibility are necessary. In particular, HA has been used as the protein repellant element to decorate polymeric surfaces (28), possibly adsorbed through polyelectrolyte complexation with polycations such as collagen (29) or chitosan (30); the formation of interfacial HA/chitosan complexes (31) is indeed the technique that we have focused on the present study.

Probably, the most popular way to produce chitosan nanoparticles is through ionotropic gelation of chitosan with sodium tripolyphosphate (TPP), a small ion with a triple negative charge throughout the physiologically acceptable pH range.

It has been initially found that concentrations below 2 mg/mL and 0.4 mg/mL respectively for TPP and chitosan, should be used, in order to avoid the formation of large aggregates, with chitosan/TPP mass ratios possibly not exceeding 15–20/1 (32); larger chitosan/TPP ratios yielded particles with larger size (but obviously lower cross-linking density) and zeta potential (32,33). Kumacheva *et al*. have refined these initial studies, investigating the effect of chitosan fractional precipitation and deacetylation as means to increase its TPP-binding efficiency (34).

We have here expanded the findings of Kumacheva, using a highly deacetylated chitosan and focusing on the different variables that may affect the chitosan–TPP complexation: not only chitosan/TPP mass ratio, but also pH, which determines chitosan protonation degree and therefore both its binding ability and its self-association, and volume ratio between the solutions. The latter parameter is of often neglected significance: if the complexation kinetics is of the same order of magnitude as or quicker than the mixing of the two solutions, the factors influencing the latter (e.g. the volume ratios between the solutions) will strongly influence the structure of the nanoparticles.

Specifically, we have screened the above parameters with the aim to a) obtain a narrow size distribution, possibly peaked at a size that allows sterile filtration (markedly below 500 nm); b) high and positive zeta potential, to provide both electrostatic stabilisation and the possibility of depositing the surface a negatively charged polyelectrolyte, such as HA; c) stability of both size and zeta potential in water and/or buffer, in order to ensure long-term storage.

We have then studied the conditions for the adsorption of hyaluronic acid (HA) on the nanoparticle surface, with the aim to present a negative Zeta potential (→electrostatic stabilisation), a "stealth" character (→prolonged circulation time) and possibly target HA receptors, while preserving the pH dependence and the endosomal disruption activity of chitosan.

Both uncoated and HA-coated nanoparticles (a sketch of the latter type is provided in Fig. 1) have been characterized for their cytotoxic effects on two model cell lines: non-phagocytic fibroblasts and phagocytic macrophages, discussing their effects on cell viability and on the integrity of cell membranes.

EXPERIMENTAL

Materials

Pentasodium triphosphate (Fluka), 1 N hydrochloric acid, DMSO, 1 N sodium hydroxide (Aldrich), MTT reagent (Sigma), glacial acetic acid (VWR BDH Chemicals) were used as received. 10 mM PBS was prepared from appropriate tablets (Oxoid, Basingtoke, UK). Chitosan ("low MW": Cat. No. 448869, Aldrich) was used after purification as described hereafter. Hyaluronic acid with average viscosimetric molecular weight of $15*10^3$ g/mol and $360*10^3$ g/mol was obtained from Medipol (Lausanne, Switzerland).

Physico-chemical Characterisation

Dynamic Light Scattering (DLS) and zeta potential measurements were performed on a Zetasizer Nanoseries ZEN3600 (Malvern Instruments) equipped with a solid state HeNe laser (λ=633 nm). All the samples were analyzed at an angle of 114° and a temperature of 25°C. AFM measurements were performed on nanoparticles deposited on a mica surface by room temperature drying of diluted dispersions in deionised water; a Molecular Force Probe 3D AFM (MFP-3D, Asylum Research, Santa Barbara, CA) equipped with a 90 μm scanner and silicon cantilevers (model AC-240, Olympus; spring constant 2 N/m) was employed in tapping mode and with a scan rate of 1 Hz. Viscosity measurements were performed on a 0.25 M acetic acid/0.25 M sodium acetate solution using a falling ball automated microviscometer (Anton Parr) at 25°C equipped with a 1.6 mm internal diameter capillary tube at an inclination angle of 30°C. The visosimetric average molecular weight was calculated assuming the parameters of the Mark-Houwink equation to be equal to $K=1.57\times10^{-5}$ L.g^{-1} and $a=0.79$ (35).

^{1}H-NMR spectra were recorded on JEOL EX270 270 MHz NMR spectrometer (Bruker Avance 270, Coventry, UK). Infrared spectra were recorded on a Tensor 27 in ATR mode. UV-Vis spectra were recorded on a Perkin Elmer Lambda 850 spectrometer.

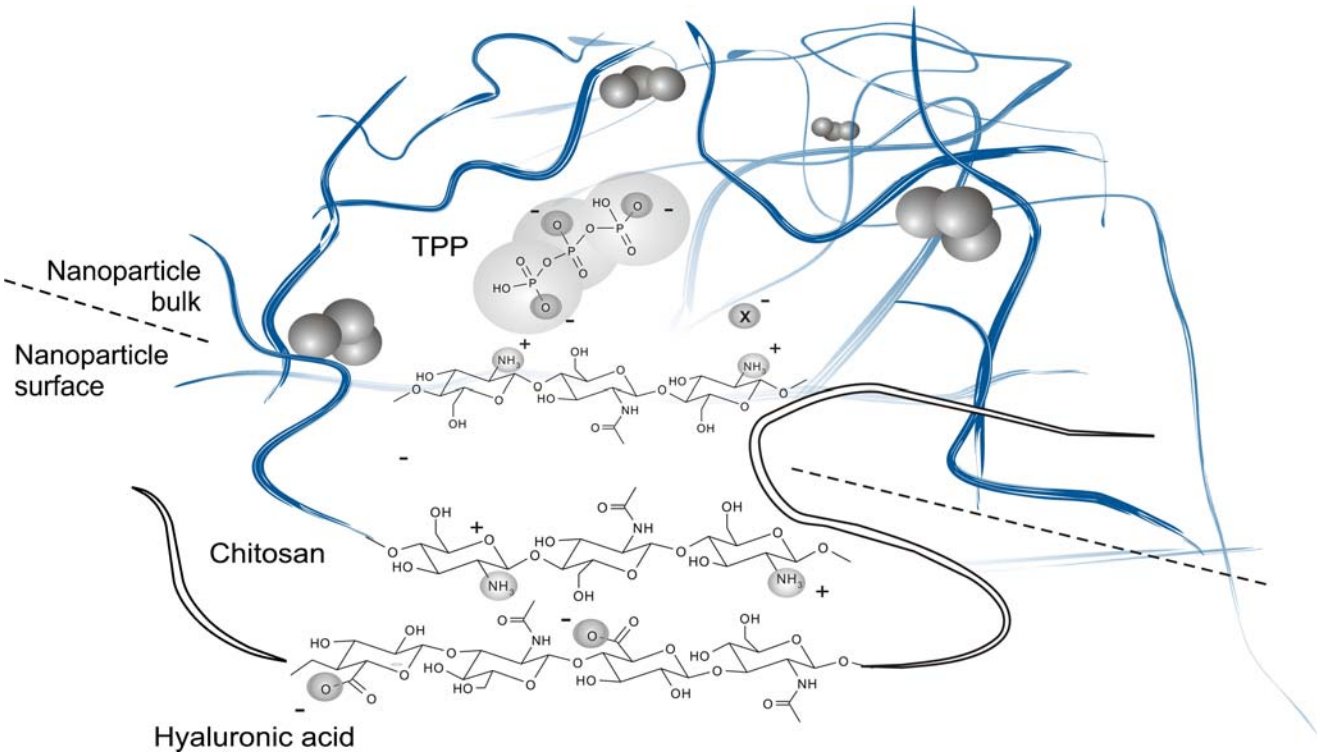

Fig. 1. Graphical view of the HA-coated chitosan/TPP nanoparticles: TPP is present in the bulk of the nanoparticles bridging between positive charges of the chitosan chains. The negatively charged HA on the other hand binds chitosan on the surface of the nanoparticles, although a certain degree of diffusion in the bulk is possible.

Preparative Procedures

Purification of Chitosan

5 g of chitosan were dissolved in 400 mL of a 2% w/v acetic acid solution in double distilled water. Complete dissolution was achieved after 16 h of stirring. The solution was then boiled for 15 min in order to denature and precipitate any proteic contaminant.

The mixture was then centrifuged for 10 min at 4500 rpm, the supernatant was removed then and filtered through 1 μm pore size filters. The pH of the solution was then corrected to 9 with 1 N sodium hydroxide, in order to precipitate chitosan from the aqueous phase. After centrifugation, the precipitate was redispersed and again sedimented via centrifugation twice, always using water at pH=9 as a dispersing medium. The procedure was repeated with Millipore water until the pH and conductivity values reached the values of pure water. The sample was freeze-dried (yield of the overall procedure=86%) and stored at 4°C.

^{1}H-NMR (2%w/w HCl/D_2O): δ=2.3–2.4 (acetamide CH_3), 3.4–3.6 (CH-NH_2), 3.8–4.4 (two broad peaks comprising CH-$NHCOCH_3$ and all other non-anomeric protons), 5.15–5.3 (anomeric protons) ppm.

ATR-IR (thin film): 3500–3000 (ν OH and NH_2), 2875 (ν CH), 1647 (amide I), 1588 (amide II) 1380, 1320, 1063, 1030 cm^{-1}.

Colloid titration was performed in a 0.02 M acetate buffer/0.1 M NaCl at pH 4.5, which was used as the solvent for chitosan and poly(styrene sulfonate) (PSS) and toluidine blue (a cationic metachromatic indicator). 2 ml of $5*10^{-3}$ mg/ml chitosan solution were added of 20 μl of 0.03% toluidine blue O solution and then titrated with a PSS solution $1*10^{-3}$ M in sulfonate groups, recording the ratio of the absorbance values at 635 and 600 nm.

Degree of deacetylation: before purification 92.02 mol % (^{1}H-NMR: ratio between acetamide protons and anomeric protons), 87.5 mol % (IR: ratio between the absorbance values at 1655 and at 2875 cm^{-1}), 91.2 mol % (colloid titration); after purification: 91.01 mol % (^{1}H-NMR), 85.4 mol% (IR), 89.7 mol % (colloid titration).

Intrinsic viscosity and viscosimetric average molecular weight: before purification $[\eta]$=0.493 L/g, Mv=$492*10^3$ g/mol; after purification $[\eta]$=0.481 L/g, Mv=$477*10^3$ g/mol.

Assessment of protein content: 10 mL of a 2% wt. solutions in 0.1 M HCl of unpurified and purified chitosan were added of 1 mL of 1 M NaOH to provoke complete precipitation; after centrifugation at 4500 rpm for 50 min the supernatant was collected and analysed with a QuantiPro kit in a Biotek© Synergy multiplate reader: 100 μL of the supernatant or of albumin solutions of different concentration were added of 100 μL of QuantiPro Working Reagent and incubated at 37°C for 2 h, reading the absorbance at 562 nm. The concentration of proteins in the unpurified and purified samples were measured to be, respectively, 19.0 μg/mL and 10.2 μg/mL, which correspond to 1.056 mg and 0.561 mg of protein per gram of dry chitosan.

Preparation of Chitosan-TTP Nanoparticles

Chitosan was dissolved in 4.6 mM HCl at concentrations 0.038%, 0.054%, 0.069%, 0.085% and 0.1% wt.adjusting the pH of the different solutions to 3, 4, 4.5 or 5 by the addition of appropriate volumes of NaOH 0.1 M. All solutions were sonicated for 40 min.

TPP was always prepared as a 0.1% wt. solution in deionised water, correcting the pH with appropriate additions of HCl 0.1 M.

Both solutions were filtered through a 0.22 μm pore size filter and, in order to remove any macroscopic material possibly present (however, freeze drying equal volumes of solution of purified chitosan before and after filtration provided the same weight of material, ensuring the precise knowledge of the polymer concentration). The complexation was then carried out at 25°C and under magnetic agitation (750 rpm) for a duration of 30 min, followed by sonication for 40 min, leaving then the dispersion undisturbed for additional 16 h prior to any purification (ultrafiltration through 500 kDa molecular weight cut-off polyethersulphone (PES) membranes) or analysis. Dispersions with different nanoparticle content could be obtained by concentrating the dispersions during ultrafiltration and assessing their concentration by measuring the dry content after freeze drying.

Method A: variable chitosan concentration, constant volumes of solution. 2.786 g of a chitosan solution with concentration 0.038, 0.054, 0.069, 0.085 or 0.1% wt. and pH= 3, 4, 4.5 or 5 were mixed with 214 mg of a 0.1% wt. TPP solution at the same pH; in alternative a chitosan solution with one of the above concentrations and pH=4 was mixed with a 0.1% wt. TPP solution at pH=8.

Final concentrations: chitosan=0.035, 0.050, 0.064, 0.079 or 0.093% wt., TPP=0.0071% wt., corresponding to 5/1, 7/1, 9/1, 11/1 or 13/1 mass ratios between the two components.

Method B: constant chitosan concentration, variable volumes of solution. A 0.1% wt. chitosan solution at pH=3, 4, 4.5 or 5 was mixed with a 0.1% wt. TPP solution at the same pH, or, in alternative, the chitosan solution at pH=4 was mixed with the TPP solution at pH=8, according to the following mass ratios and for a total mass of 3 g: 2786/214, 2750/250, 2700/300, 2625/375 and 2500/500.

Final concentrations: chitosan=0.083, 0.088, 0.090, 0.092 and 0.093% wt. TPP=0.0071, 0.0083, 0.0100, 0.0125, 0.0167% wt., corresponding to 5/1, 7/1, 9/1, 11/1 or 13/1 mass ratios between the two components.

Characterisation: the nanoparticles were characterised by measuring size, Zeta potential and morphology (AFM). Due to TPP low concentration, IR analysis did not reveal any peak typical of phosphate groups; it is therefore generally assumed the chitosan/TPP ratio to be the same as in the feed.

In the evaluation of the nanoparticle dispersity in size, we have compared the aspect ratios of the distribution, which were obtained dividing the width at half height by the peak value. We have followed the same approach for multimodal distributions, using the size of the largest peak and the overall width of the distribution.

The peak values of the zeta potential data are often very close to zero and therefore very low aspect ratios are obtained also for narrow peaks; therefore the breadth of the zeta potential distributions was evaluated just on the basis of the width at half height of the peaks.

Coating of Chitosan-TTP Nanoparticles with Hyaluronic Acid

Chitosan /TPP nanoparticles ("small" nanoparticles, method A, pH5-pH5, CS/TPP 9:1, Z av. size 240 nm, Zeta potential=43.9 mV) were dispersed in a 100 mM acetic acid/acetate buffer at pH=5 at a concentration of 0.05 or 0.1% wt. 2 mL of these dispersions were slowly added under vigorous stirring (30 min, 1200 rpm) to an equal amount of acetate buffer of equal strength containing hyaluronic acid of molecular weight $15*10^3$ g/mol and $360*10^3$ g/mol at a concentration of 0.05%, 0.10%, 0.15%, 0.20% or 0.50% wt. The dispersions were then purified via ultrafiltration using a 500 kDa cut off membrane, and concentrated up to 0.30% w/w.

Cell Culture and Cytotoxicity Assays

Murine fibroblasts L929 and macrophages J774.2 (ECACC, UK) were maintained as, respectively, adherent and semi-adherent cell culture at 37°C in humidified atmosphere (5% CO2) in Dulbecco modified Eagle's minimal essential medium (DMEM, 25 mM glucose) supplemented with 2 mM glutamine (Gibco), 10% heat inactivated fetal calf serum (FCS) (Invitrogen, UK), 100 IU/ml penicillin and 100 IU/ml streptomycin (Gibco). For fibroblasts L929 cells splitting, trypsin-EDTA (Invitrogen, UK) consisting of 2.5% (w/v) of trypsin and 0.2% (w/v) EDTA in PBS was used while macrophages J774.2 cells were detached by scraping. For experiments, both cell lines were adjusted to the required concentration of viable cells, by counting in a haemocytometer in the presence of 0.4% trypan blue.

The nanoparticles used for cytotoxicity experiments were purified by dialysis in PBS (10 mM, pH 6). Once reached the equilibrium in conductivity between filtrate and PBS solution the samples were concentrated to the appropriate concentration in an ultrafiltration cell. In each step the size and z-potential was checked by DLS.

The MTT assay measures the cell metabolic activity whereby the mitochondrial dehydrogenase enzyme of viable cells reduces the yellow tetrazolium salt, 3-[4,5-dimethylthiazol-2-yl]-3,5-diphenyl tetrazolium bromide dye (MTT), to a purple formazan crystals (36–38). Macrophages J774.2 and fibroblasts L929 cells were seeded in 96-well plates at 10,000 cells per well in complete medium containing 10% FCS. The cytotoxicity of the nanoparticles was evaluated using the MTT assay by determining the cells viability after for 24 h incubation with different concentrations of hyaluronic acid-coated or uncoated chitosan nanoparticles. A shorter time of 4 h incubation was used for the two-temperature comparison tests run at 4°C and 37°C, since longer incubation times at low temperature cause a drastic decrease in cell viability also in the absence of nanoparticles. At the end of the incubation period in the presence of nanoparticles, cells were washed three times with PBS pH 7.4 and incubated with 100 μl of a MTT solution (0.5 mg/ml in DMEM) for 4 h at 37°C. One hundred microliters of dimethyl sulfoxide (DMSO) were then added to dissolve the formazan crystals. The UV absorbance of the solubilized formazan crystals was measured spectrophotometrically (Microplate reader, TECAN, Safire, Austria) at 550 nm. Cell viability was expressed as the ratio between the absorbance reading for cells treated with the different nanoparticles and for control non-treated cells. The concentration inhibiting cell viability by 50% (IC50) was obtained by interpolation of the cell viability curves (39,40).

The LIVE/DEAD double staining kit (Sigma, St Louis, MO, USA), which allows the simultaneous fluorescence staining of viable (Calcein-AM, excitation 495 nm, emission 515 nm) and dead (Propidium iodide, PI, excitation: 535 nm, emission: 617 nm) cells (41,42), was used. Macrophages J774.2 were seeded in a 96-well plate at a count 8,000 cells/well and incubated for 24 h with 0.1 mg/ml of coated or uncoated CSNPs. After removal of the two treatments, cells were washed with PBS, incubated with solution of both stains for 15 min at 37°C and then observed under fluorescent microscope (Leica DMI5000,) at 20-fold magnification. Both Calcein-AM and PI-DNA were excited with 490 nm, allowing simultaneous monitoring of viable and dead cells while with 545 nm excitation, only dead cells were observed. In order to quantitatively assess the data obtained from the fluorescent images, the total number of cells and number of dead cells in three microscopic fields were counted (ImageJ 1.4d, USA) such that each microscopic filed contains around 300–360 cells. Each NPs formulation was assayed at least in triplicate wells.

Statistics. All experimental results are expressed as mean ± SD. Statistical tests of significance were performed using one-way ANOVA followed by Bonferroni test for multiple comparisons at $P<0.05$ (Origin® 7SR1, Northampton MA, USA).

RESULTS AND DISCUSSION

Purification of Chitosan

In this study we have used chitosan with high degree of deacetylation (≈90%), employing a precipitation-redissolution procedure for removing contaminants, which are supposedly, but not necessarily, of proteic nature. The process did not modify the degree of deacetylation, which was evaluated

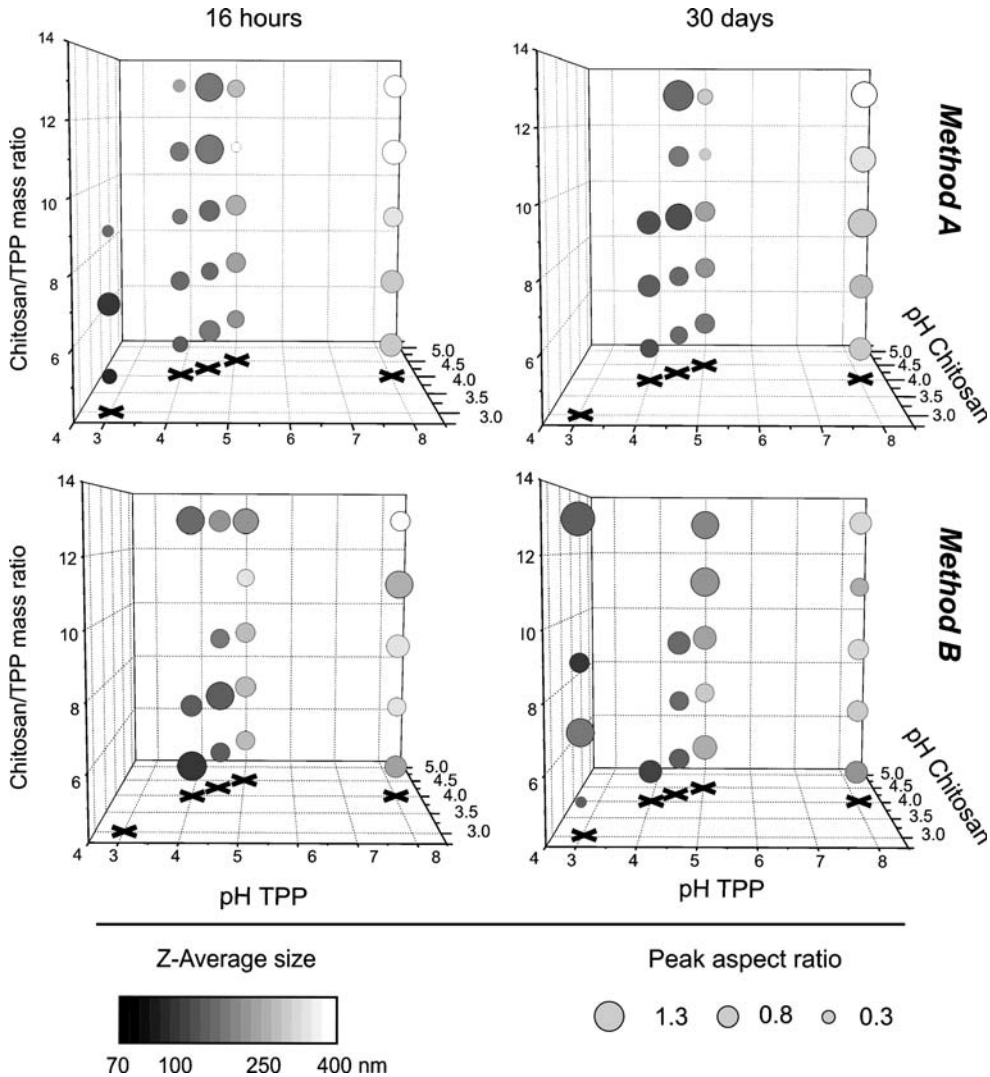

Fig. 2. Average size and aspect ratio of the size distributions (average over three different preparations) as a function of chitosan/TPP mass ratio and pH of both solutions. Above; mixing method A (volume ratio kept constant); below: mixing method B (concentrations kept constant). The pH combinations are highlighted with black crosses at the bottom of graphs. Samples with very low scattered intensity (corresponding to entirely soluble, very small or extremely polydisperse materials) were excluded from the graphs. A representative size distribution curve is shown in Fig. 2 of the Supporting information.

through ^{1}H-NMR, IR and colloid titration, nor the intrinsic viscosity of the polymer, but removed a significant amount of contaminants in form of soluble proteins or colloidal impurities, which are capable of significantly affect both the process of nanoparticle formation and the interactions with cells.

As a qualitative measure of the efficacy of the purification procedure, the amount of base-soluble proteins is reduced to about 0.05% wt. of the chitosan mass (roughly 50% of the initial base-soluble protein content): this would correspond to a protein content of 0.5 ppm for a 0.1% chitosan concentration, a protein level that was deemed acceptable for further use.

Preparation of Chitosan/TPP Nanoparticles

Chitosan and TPP were used at relatively high dilution (0.035–0.093% and 0.007–0.017%, respectively) in order to avoid the formation of large aggregates.

Having as a target the preparation of nanoparticles with a high and positive Zeta potential (for allowing the effective adsorption of a polyanion at a later stage), dimensions in the range 100–400 nm, and a long-term stability of both size and charge, we have conducted a semi-combinatorial optimization of the preparative process, monitoring the average value and the dispersity of size and zeta potential, as well as the stability of these values and of pH at 16 h 30 days after complexation.

Specifically, we have investigated the influence of the following mutually independent (orthogonal) variables: chitosan/TPP mass ratio, pH of both solutions and nature of the mixing procedure.

Chitosan/TPP mass ratio. Since an excess of chitosan is necessary to provide positively charged particles, this ratio is inversely related to the cross-link density of the material. A large chitosan/TPP ratio therefore, corresponding to a low

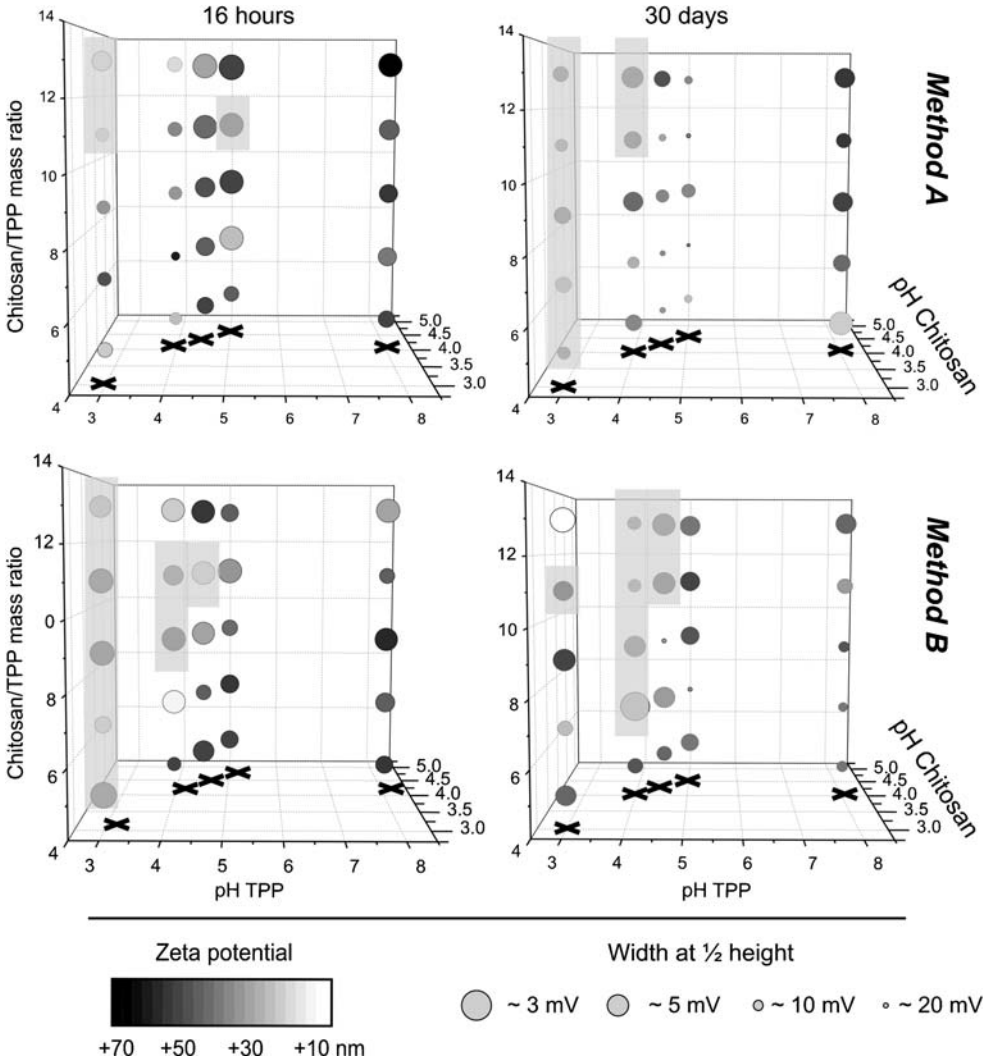

Fig. 3. Average Zeta potential and width at half height for the Zeta potential distribution (average over three different preparations) (average over three different preparations) as a function of chitosan/TPP mass ratio and pH of both solutions. Above; mixing method A (volume ratio kept constant); below: mixing method B (concentrations kept constant). The pH combinations are highlighted with black crosses at the bottom of graphs. Low scattering samples (excluded from Fig. 2) are overlayed in grey and the corresponding values of Zeta potential have to be considered just qualitative. A representative Zeta potential distribution curve is shown in Fig. 2 of the Supporting information.

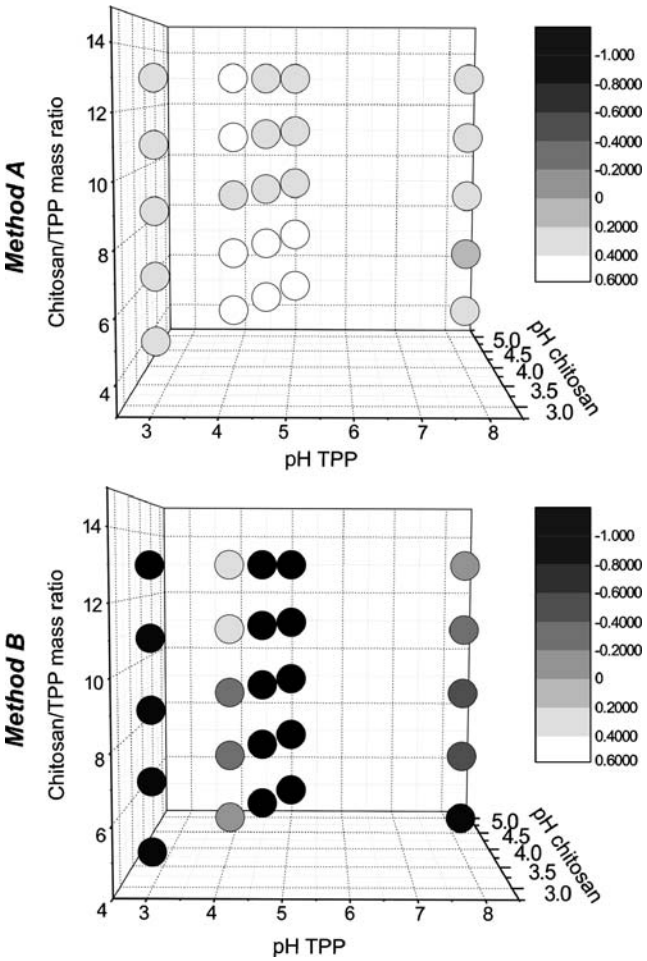

Fig. 4. pH stability of the dispersions presented in Figs. 2 and 3, expressed as the difference between the pH values at 16 h and 30 days.

cross-linking density, provides a softer materials, but also possibly a slower kinetics of formation, which may mean a more controlled process of formation. Specifically, we have varied the mass ratio between 5:1 and 13:1.

pH. While at pH<4 TPP charge drops below 3, decreasing its cross-linking capability, at pH>6 the decrease in chitosan charge density lowers not only the intensity of its electrostatic interactions, but also its solubility in water. We have therefore performed most complexation experiments mixing TPP and chitosan solutions with an identical pH, with values ranging between 3 and 5. We have explored an alternative mixing procedure with acidic (pH=4) chitosan and a slightly basic (pH=8) TPP: the transient exposure to a higher pH may induce some chitosan aggregation, increasing the number of nuclei available for nanoparticle growth (higher nucleation rate → smaller particles).

Mixing process. Method A: constant volume ratio but variable concentration of the two solutions. Method B: variable volume ratio but constant concentration (0.1% for both TPP and chitosan). Assuming viscosity to be constant, due to the high dilution, the mixing process of samples with the same amounts of chitosan/TPP concentration and pH should strongly depend on the volumetric ratio of the solutions. If the kinetics of chitosan/TPP complexation comparable or quicker to that of mixing, i.e. if it starts happening before complete mixing, the two methods are expected to provide different materials.

Fig. 2 summarises the influence of the above variables on the nanoparticle size: the darker the colour, the smaller the nanoparticle size, while the larger the circle, the narrower the distribution. In Fig. 3 analogously darker colour corresponds to higher zeta potential, while larger symbols correspond to narrower distributions. In the essence, in both figures the most interesting conditions correspond to symbols with darker colour and larger size. Through a similar 3D graph Fig. 4 presents the pH variation of the dispersions stored for 16 h and for 30 days.

The two mixing methods provided largely different results, indicating a substantial kinetic control on the complexation; generally, method B provided more frequently very polydisperse samples. Additionally, the nanoparticles clearly evolved with time, more frequently shrinking; this effect could be due to a slow increase in cross-linking density: the presence of a multiply charged and immobilised anion, such as TPP, is likely to increase the protonation of neighbouring amines (the basicity of chitosan primary amines increases with the number of immobilized negative charges present nearby). Leading to an increase in both cross-linking density and pH. Indeed, while the pH of the dispersions obtained through method A is substantially stable, a clear increase up to one pH unit was seen for method B, therefore suggesting a less controlled nature of the complexation with this method.

In terms of the effects of pH, it is recognizable that: a) the larger size of the nanoparticles obtained using a higher pH in the TPP solution is likely a consequence of chitosan aggregation when exposed to mildly basic pH; the nanoparticles were, however, not simply composed by aggregated chitosan since they were not re-dissolved under mildly acidic conditions. B)

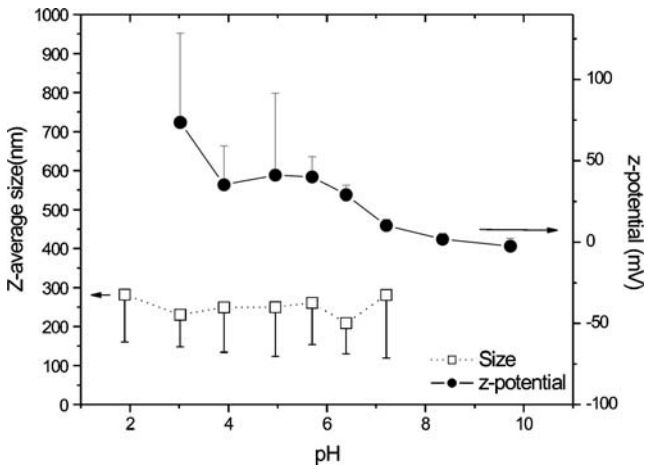

Fig. 5. Dependence of the z-average size and of the Zeta potential on the pH for the "large" nanoparticles. A similar depdence is recorded for the "small" nanoparticles. It is worth mentioning that the data were obtained by adding appropriate quantities of HCl or NaOH to the nanoparticles originally at pH=5.5, without the use of any buffer.

Generally, experiments conducted at pH=3 produced very low amounts of nanoparticles, due to the decreasing charge density of TPP with decreasing pH (TPP's pKa_3=2.3, therefore at pH=3 around 20% of its molecules are only double charged).

The average Zeta potential was always largely positive, with reasonably narrow distributions fully comprised within the positive potential region. No specific dependence could be highlighted for samples produced through method B; for method A, lower pH seemed to cause broad dispersity immediately after preparation, narrowing down after 30 days; the variability of these data is, however, fairly large and it is difficult to conclusively ascribe this effect to a specific phenomenon. It is noteworthy that within the pH range used for the production of stable particles (between 4 and 6), the Zeta potential did not show any sound dependence on pH.

Finally, high chitosan/TPP ratio seems a detrimental factor too, likely due to the low cross-linking density.

Selection of optimised nanoparticles. Due to the generally poorer results in terms of scattering intensity and/or polydispersity, method B was then discarded for further studies. Seeking the best combinations of stability (of size, Zeta potential and pH), high Zeta potential and narrow size dispersity, we have therefore focused our attention on two samples characterized by a "small" (200–300 nm in deionised water) or a "large" (300–400 nm) size. Since the process of coating with hyaluronic acid is very likely not only to modify the nanoparticle surface, but also to increase their size, we have employed the "small" nanoparticles for coating experiments and the "large" ones as a reference system, similar in size and bulk composition to the coated ones, but displaying a chitosan-based surface.

Specifically, the "small" nanoparticles, were prepared at pH=5 for both solutions, chitosan/TPP 9:1, Z-average size 240 nm, Zeta potential=43.9 mV. The "large" nanoparticles, at pH=4/8, CS/TPP 13:1, Z-average size 360 nm, Zeta potential=47.0 mV

Environmental Effects on Chitosan/TPP Nanoparticles

Due to protonation of TPP, acids are detrimental to nanoparticle stability. Indeed at pH≤3 the scattering intensity drastically decreases and zeta potential cannot be any longer reliably determined (Fig. 5), indicating a substantial dissolution. At pH>6, on the other hand, the Zeta potential gradually approaches neutrality and agglomeration and macroscopic flocculation occurs

In order to ensure long-term stability to the nanoparticle dispersions, the use of buffers in the 4–6 pH region appears the most logical solution. On the other hand, the resulting high concentration of ionic species and the high osmotic pressure may on its turn influence the nanoparticle morphology and/or stability. Indeed upon exposure to moderate or high ionic strength buffers, the nanoparticles show a sound reduction in size to 62–68% the original average diameter, corresponding to a shrinkage to roughly one third of the initial volume. The extent of the shrinkage was substantially analogous in 10 mM PBS at pH=6 (Fig. 6) and in 100 mM acetate at pH=5, with a negligible influence on the Zeta potential in both cases.

Hyaluronic Acid-coated Nanoparticles

The adsorption of a polyanion on positively charged nanoparticles can result in agglomeration and possibly flocculation, either because of the interactions between positively and negatively charged patches on different nanoparticles, or because of the absence of electrostatic stabilization during the intermediate states of the adsorption.

The final outcome, i.e. surface functionalisation or agglomeration, depends on the concentration and size of both nanoparticles and polyanion and on the strength of their interactions. Since the last parameter is automatically set by the choice of materials (interactions between ammonium ions and carboxylates) and pH (5 to ensure both stability of the initial chitosan nanoparticles and sufficient deprotonation to HA), we have studied the influence of the other parameters, limiting our investigation to relatively dilute systems, in order to minimize the chance of aggregation, to two HA molecular weights ($15*10^3$ g/mol and $360*10^3$ g/mol). Very high molecular weight HA was excluded, on the grounds that the high viscosity of its solutions could result in scarcely reproducible experiments.

Only "small" nanoparticles were coated with HA, using the uncoated "large" nanoparticles, only as a reference to highlight effects arising only from surface composition.

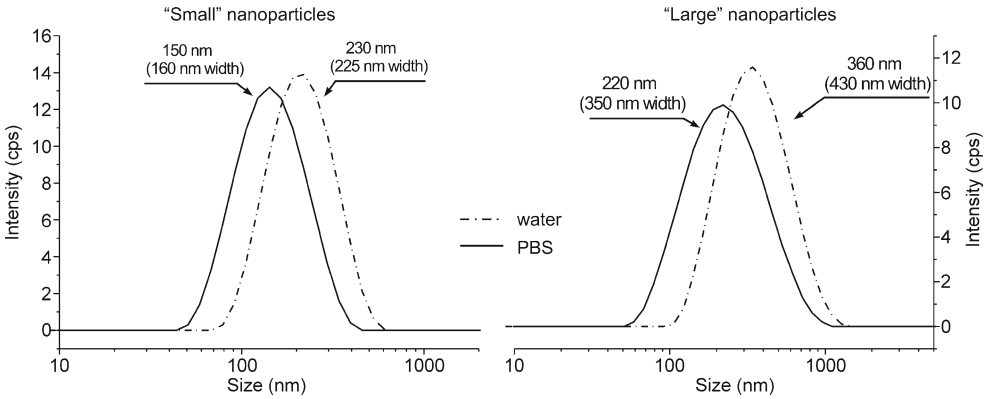

Fig. 6. Changes in the size distribution of "small" and "large" chitosan/TPP nanoparticles as a consequence of the exchange of the medium from deionised water to 10 mM PBS.

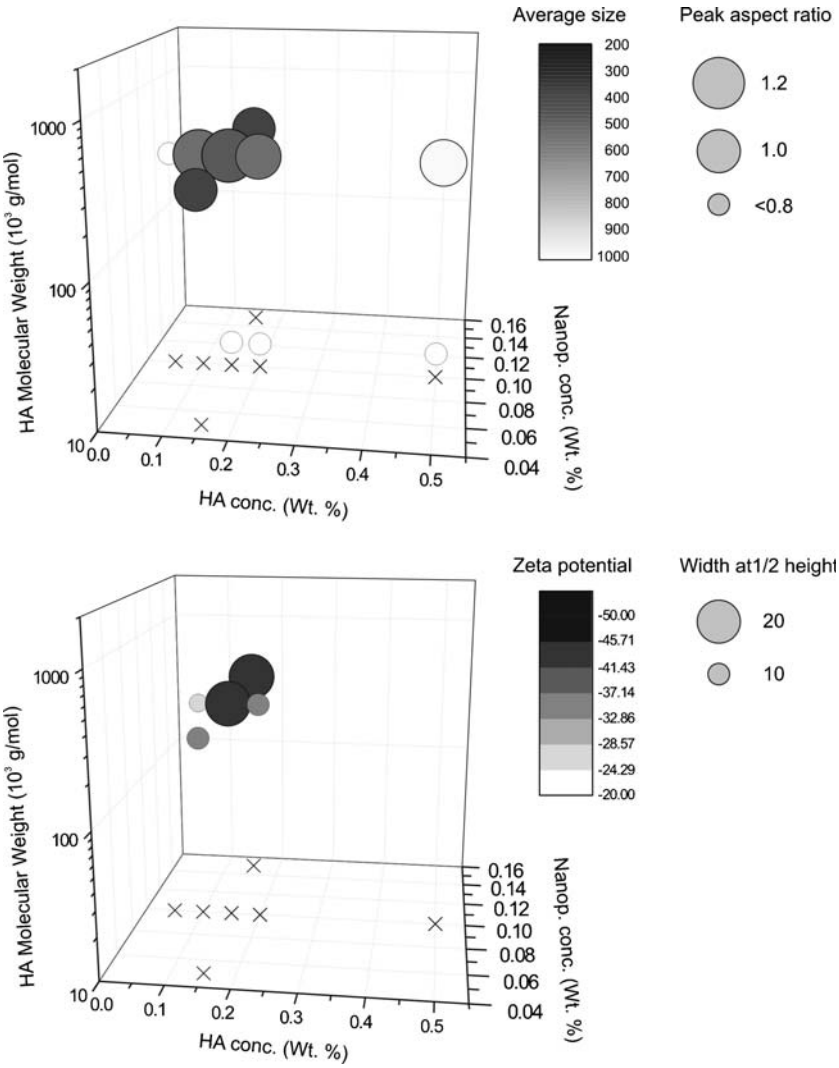

Fig. 7. Average size and aspect ratio of the size distributions (top) average Zeta potential and width at half height for the Zeta potential distribution (bottom) as a function of nanoparticle and HA concentration. For an easier reading, the concentration values are highlighted with black crosses at the bottom of graphs.

Our experiments have shown that low molecular weight HA appeared to be detrimental to the stability of the nanoparticles (Fig. 7). Low polydispersity and reasonably low size increase was on the contrary recorded for HA of MW=360*10^3 g/mol at concentrations comprised between 0.1% and 0.2% wt.

The lowest polydispersity and the smallest size increase (average size=260 nm in acetate buffer, compared to 160 nm before adsorption) were recorded for the combination of "small" nanoparticles at 0.05% wt. and HA at 0.15% wt. These optimised HA-coated nanoparticles are likely the result of a moderate agglomeration, with an individual volume roughly corresponding to that of 3–4 "small" nanoparticles.

A morphological comparison of the three different kinds of nanoparticles through Atomic Force Microscopy (Fig. 8) showed that A) the dimensional difference between "large", "small" and HA- nanoparticles is real and not an artifact of the DLS analysis. It is noteworthy that the HA-coated nanoparticles, although likely obtained through the agglomeration of few "small" ones, do not appear as clusters. B) all nanoparticles are soft and flatten when deposited on a solid surface. C) Both "Large" and HA-coated nanoparticles generally show some fracture lines as a consequence of drying, which suggests them to display a harder surface. "Small" nanoparticles appear to be always surrounded by a halo, which is barely visible in height images but more clear in phase images (not shown), indicating it to be very soft and thin; we interpret it as a "fuzzy" corona composed by tethered chitosan chains. Consistently with this hypothesis, the halo disappears after coating.

Evaluation of Nanoparticle Cytotoxicity

Cytotoxicity was evaluated on two murine cell lines: J774 macrophages as a model for professional phagocytes

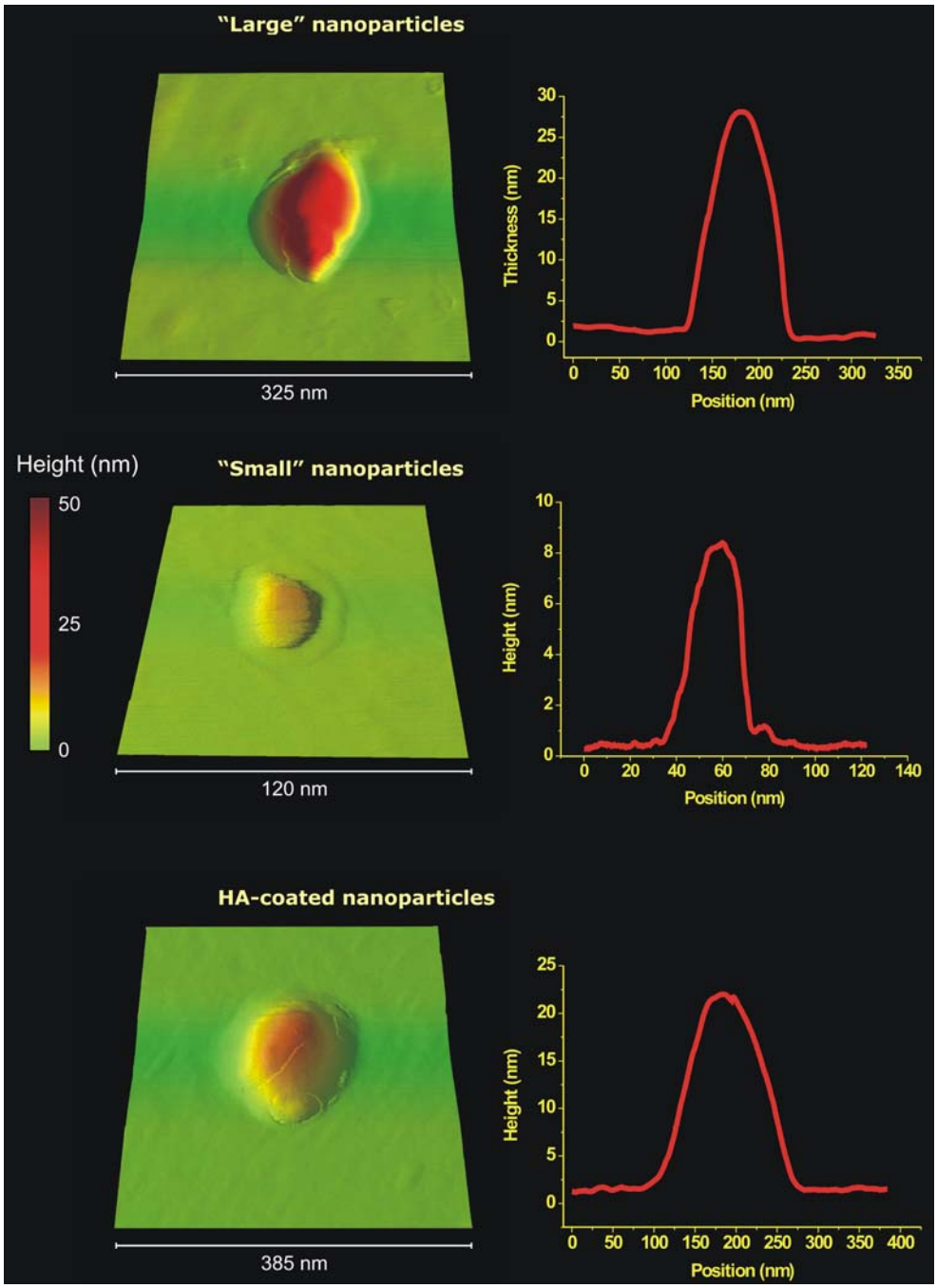

Fig. 8. AFM analysis of the three different kinds of nanoparticles deposited on mica surfaces from dispersions in deionised water. The lower (*left*) or higher (*centre*) magnification pictures and the height scans along the median point of particles (*right*) highlight the larger dimensions of "large" and HA-coated nanoparticles compared to the "small" ones.

(43–45) and L929 fibroblasts as a non-phagocytic and widely recommended reference cell line (46). Two methods were employed: the MTT (3-(4,5-dimethylthiazol-2- yl)-2,5-diphenyl tetrazolium bromide) assay to evaluate the effects that nanoparticles may have intracellularly on mitochondria and metabolic activity and determine IC50 values for the above nanoparticles, and a Live/Dead fluorimetric assay (calcein/propidium bromide) to assess not only cell death, but also possible non-lethal cell membrane damage, since the first site of interaction of nanoparticles is likely to be the cell membrane (39,47). The combination of these two different methods can provide hints about the *modus operandi* of the nanoparticle toxicity, since effects may appear at lower concentrations or shorter times than those recorded through the measurement of mithocondrial activity.

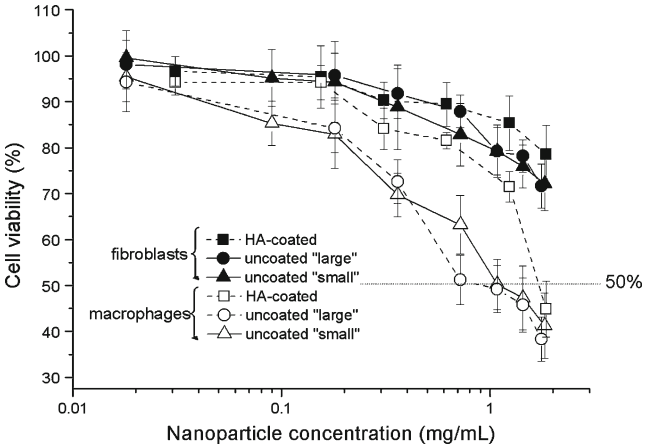

Fig. 9. Cell viability (MTT assay) for L929 fibroblasts and J774 macrophages as a function of nanoparticle concentration at 37°C after 24 h exposure.

The results of the MTT assay (Fig. 9) clearly show that

- for all nanoparticles and at any concentration, cytotoxicity was always higher for macrophages than for fibroblasts. Specifically, the decrease in viability recorded on fibroblasts is still small also at concentrations as high as to 2 mg/ml.
- Using macrophages as a more sensitive model, it is also apparent that the uncoated, positively charged nanoparticles have higher cytotoxicity than the HA-coated ones. "Large" and "small" nanoparticles show IC50 values in between 0.7–1.0 mg/ml; although "small" nanoparticles often show higher cell viability than the "large" ones, the data offer no statistically significant difference. The HA-coated nanoparticles on the contrary show a higher IC50 of about 1.8 mg/ml.
- The more benign character of the HA-coated nanoparticles is also revealed by the Live/Dead assay at concentrations where the MTT assay still indicates no significant decrease of viability (0.1 mg/mL). "Large" nanoparticles produce a fraction of membrane-damaged cells which is considerably higher than for the HA-coated ones, which on its turn is almost undistinguishable from the control (Fig. 10; for a quantitative evaluation see Table 1 in Supporting information). It is noteworthy that red and green emissions are not co-localised and that there is a considerable number of cells with low green emission, but no red one. This is likely an indication that membrane damage, i.e. penetration of the red-emitting propidium iodide in the cell, takes place only after a sound decrease of the cell metabolic activity. Therefore, even when the nanoparticles are positively charged, they appear to have a toxic effect directly on metabolism rather than mediated by membrane damage; we may thus conclude their cytotoxicity to be mediated by their intracellular uptake, a finding corroborated by several literature reports (48,49).

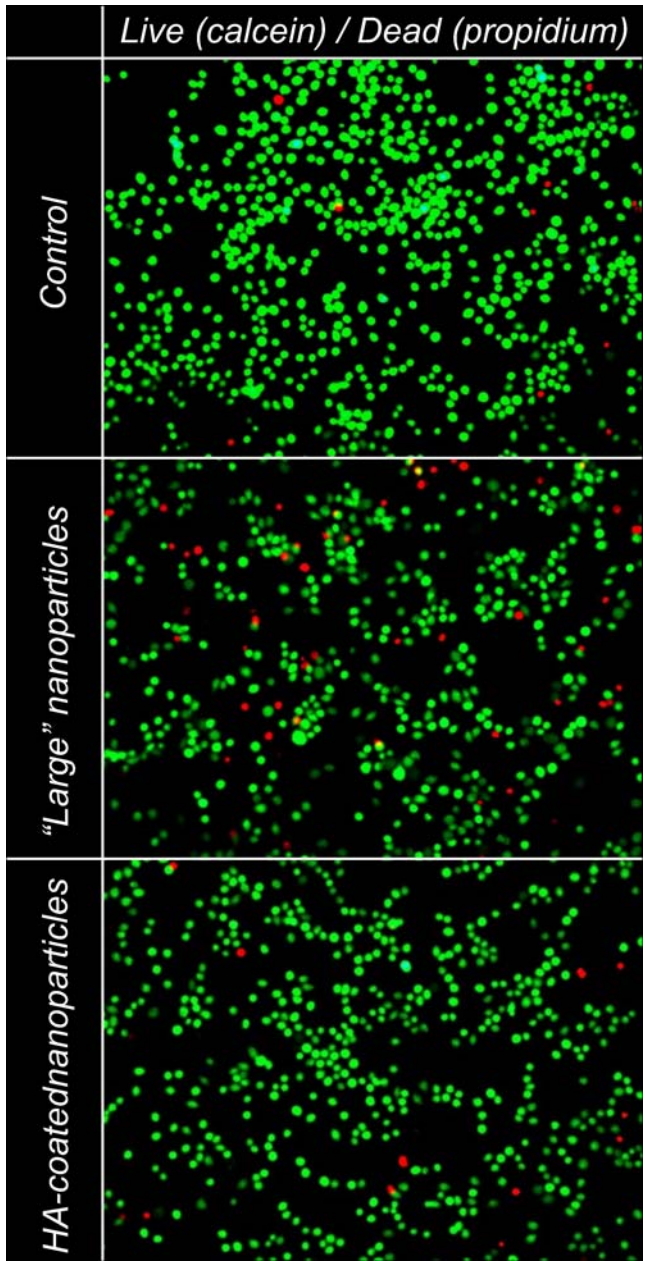

Fig. 10. Fluorescence microscopy pictures (overlaid) of metabolically active (green) and membrane-damaged (red) L929 cells. It is apparent that while pure culture media and 0.1 mg/mL HA-coated nanoparticles show both negligible toxic effects, a 0.1 mg/mL dispersion of the uncoated and positively charged "large" nanoparticles have a detrimental effect on the cell viability; interestingly, there is large number of cells with reduced green fluorescence, but substantially no overlap between red and green-emitting cells.

- The higher sensitivity of macrophages could therefore be due to their higher internalisation activity. This hypothesis is confirmed taking into account that membrane disruption would not be very dependent on temperature, while endocytosis is substantially inhibited at low temperature (4°C). Cytotoxicity experiments performed at different temperatures (Fig. 11) clearly showed that low temperature improves the viability of macrophages exposed to

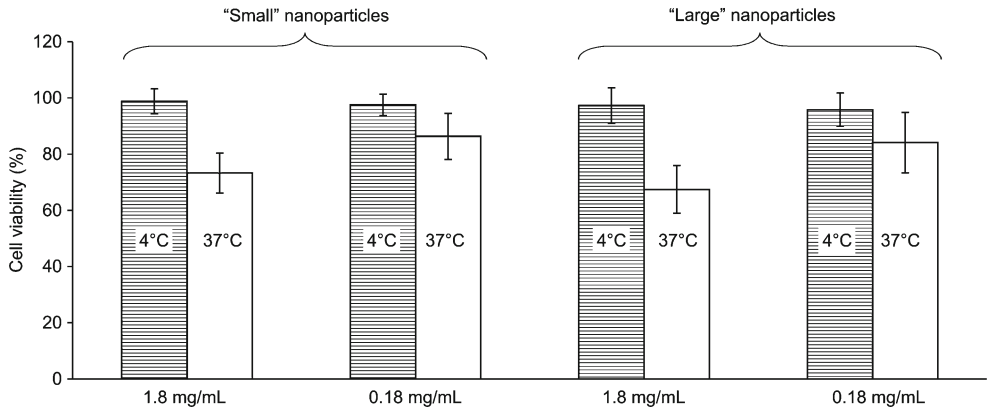

Fig. 11. Comparison of the viability (MTT assay) of J774 macrophages after 4 h exposure to uncoated chitosan/TPP nanoparticles at 4 and 37°C. It is apparent that, above all at higher nanoparticle concentrations, toxic effects disappear at low temperature.

positively charged nanoparticles, which have toxic effects at 37°C, an effect that can be related to endocytosis but not to membrane disruption.

Our data therefore suggest the cytotoxicity of chitosan nanoparticles to be mostly dependent on their internalisation, which on its turn seems to be scarcely dependent on size and clearly dominated by surface composition/charge: indeed it is well known that positively charged nanoparticles are more quickly internalised than negatively charged ones, possibly utilising clathrin-mediated mechanisms (50), where, however, interactions with membrane-linked negatively charged GAGs may play a role too (51).

Conclusions

As a result of the application of a robust approach for the optimization of the method for the chitosan/TPP nanoparticle preparation, we have focused on "small" nanoparticles with a size ≤200 nm, which were later coated with hyaluronic acid (HA), and on "large" nanoparticles with a size 200–400 nm, which can be used as a control for the HA-coated ones, featuring analogous dimensions but different surface properties. The HA-coating markedly reduces the nanoparticle toxicity; it is important to note that the lower cytotoxicity due to polysaccharidic coatings, demonstrated in the past for a number of nano-carriers, e.g. also dextran-coated nanoparticles (52), often corresponds to longer circulation times *in vivo* (53,54).

ACKNOWLEDGMENTS

The authors want to thank Dr. Philip Day (School of Translational Medicine, University of Manchester) for the helpful discussions. Financial support from EPSRC (grant No. EP/C543564/1 and Advanced Research Fellowship for NT) and from the University of Naples Federico II is gratefully acknowledged.

REFERENCES

1. Tirelli N. (Bio)Responsive nanoparticles. Curr Opin Colloid Interface Sci. 2006;11:210–6. doi:10.1016/j.cocis.2006.09.002.
2. Rehor A, Hubbell JA, Tirelli N. Oxidation-sensitive polymeric nanoparticles. Langmuir 2005;21:411–7. doi:10.1021/la0478043.
3. Brannon-Peppasand L, Blanchette JO. Nanoparticle and targeted systems for cancer therapy. Adv Drug Deliv Rev. 2004;56:1649–59. doi:10.1016/j.addr.2004.02.014.
4. Oh JK, Drumright R, Siegwart DJ, Matyjaszewski K. The development of microgels/nanogels for drug delivery applications. Prog Polym Sci. 2008;33:448–77. doi:10.1016/j.progpolymsci.2008.01.002.
5. Ganta S, Devalapally H, Shahiwala A, Amiji M. A review of stimuli-responsive nanocarriers for drug and gene delivery. J Control Release. 2008;126:187–204. doi:10.1016/j.jconrel.2007.12.017.
6. Torchilin VP. Tat peptide-mediated intracellular delivery of pharmaceutical nanocarriers. Adv Drug Deliv Rev. 2008;60:548–58. doi:10.1016/j.addr.2007.10.008.
7. Peer D, Karp JM, Hong S, FaroKhzad OC, Margalit R, Langer R. Nanocarriers as an emerging platform for cancer therapy. Nature Nanotechnology. 2007;2:751–60. doi:10.1038/nnano.2007.387.
8. Vasirand JK, Labhasetwar V. Biodegradable nanoparticles for cytosolic delivery of therapeutics. Adv Drug Deliv Rev. 2007;59:718–28. doi:10.1016/j.addr.2007.06.003.
9. van Vlerken LE, Vyas TK, Amiji MM. Poly(ethylene glycol)-modified nanocarriers for tumor-targeted and intracellular delivery. Pharm Res. 2007;24:1405–14. doi:10.1007/s11095-007-9284-6.
10. Goldberg M, Langer R, Jia XQ. Nanostructured materials for applications in drug delivery and tissue engineering. J Biomater Sci Polym Ed. 2007;18:241–68. doi:10.1163/156856207779996931.
11. Boussif O, Lezoualch F, Zanta MA, Mergny MD, Scherman D, Demeneix B, *et al.* A versatile vector for gene and oligonucleotide transfer into cells in culture and *in-vivo*-polyethylenimine. Proc Natl Acad Sci USA. 1995;92:7297–301. doi:10.1073/pnas.92.16.7297.
12. Cho YW, Kim JD, Park K. Pollycation gene delivery systems: escape from endosomes to cytosol. J Pharm Pharmacol. 2003;55:721–34. doi:10.1211/002235703765951311.
13. Murthy N, Robichaud JR, Tirrell DA, Stayton PS, Hoffman AS. The design and synthesis of polymers for eukaryotic membrane disruption. J Control Release. 1999;61:137–43. doi:10.1016/S0168-3659(99)00114-5.
14. Chen R, Khormaee S, Eccleston ME, Slater NKH. The role of hydrophobic amino acid grafts in the enhancement of membrane-disruptive activity of pH-responsive pseudo-peptides. Biomaterials 2009;30:1954–61. doi:10.1016/j.biomaterials.2008.12.036.
15. Passirani C, Barratt G, Devissaguet JP, Labarre D. Long-circulating nanoparticles bearing heparin or dextran covalently

bound to poly(methyl methacrylate). Pharm Res. 1998;15:1046–50. doi:10.1023/A:1011930127562.
16. Higuchi A, Shirano K, Harashima M, Yoon BO, Hara M, Hattori M, *et al*. Chemically modified polysulfone hollow fibers with vinylpyrrolidone having improved blood compatibility. Biomaterials 2002;23:2659–66. doi:10.1016/S0142-9612(01)00406-9.
17. Mequanint K, Patel A, Bezuidenhout D. Synthesis, swelling behavior, and biocompatibility of novel physically cross-linked polyurethane-block-poly(glycerol methacrylate) hydrogels. Biomacromolecules 2006;7:883–891. doi:10.1021/bm0507047.
18. Leeand JY, Spicer AP. Hyaluronan: a multifunctional, mega-Dalton, stealth molecule. Curr Opin Cell Biol. 2000;12:581–6. doi:10.1016/S0955-0674(00)00135-6.
19. Zhang Y, Yang M, Portney NG, Cui D, Budak G, Ozbay E, *et al*. Zeta potential: a surface electrical characteristic to probe the interaction of nanoparticles with normal and cancer human breast epithelial cells. Biomed Microdevices. 2008;10:321–8. doi:10.1007/s10544-007-9139-2.
20. Basarkar A, Devineni D, Palaniappan R, Singh J. Preparation, characterization, cytotoxicity and transfection efficiency of poly (dl-lactide-co-glycolide) and poly(dl-lactic acid) cationic nanoparticles for controlled delivery of plasmid DNA. Int J Pharm. 2007;343:247–54. doi:10.1016/j.ijpharm.2007.05.023.
21. Rehor A, Schmoekel H, Tirelli N, Hubbell JA. Functionalization of polysulfide nanoparticles and their performance as circulating carriers. Biomaterials 2008;29:1958–66. doi:10.1016/j.biomaterials.2007.12.035.
22. Etienne O, Schneider A, Taddei C, Richert L, Schaaf P, Voegel JC, *et al.* Degradability of polysaccharides multilayer films in the oral environment: an *in vitro* and *in vivo* study. Biomacromolecules 2005;6:726–33. doi:10.1021/bm049425u.
23. Agnihotri SA, Mallikarjuna NN, Aminabhavi TM. Recent advances on chitosan-based micro- and nanoparticles in drug delivery. J Control Release. 2004;100:5–28. doi:10.1016/j.jconrel.2004.08.010.
24. Katasand H, Alpar HO. Development and characterisation of chitosan nanoparticles for siRNA delivery. J Control Release. 2006;115:216–225. doi:10.1016/j.jconrel.2006.07.021.
25. Luangtana-anan M, Opanasopit P, Ngawhirunpat T, Nunthanid J, Sriamornsak P, Limmatvapirat S, *et al*. Effect of chitosan salts and molecular weight on a nanoparticulate carrier for therapeutic protein. Pharm Dev Technol. 2005;10:189–96. doi:10.1081/PDT-200054388.
26. Deng QY, Zhou CR, Luo BH. Preparation and characterization of chitosan nanoparticles containing lysozyme. Pharm Biol. 2006;44:336–42. doi:10.1080/13880200600746246.
27. Dassand CR, Choong PFM. The use of chitosan formulations in cancer therapy. J Microencapsul. 2008;25:275–9. doi:10.1080/02652040801970461.
28. Van Beek M, Jones L, Sheardown H. Hyaluronic acid containing hydrogels for the reduction of protein adsorption. Biomaterials 2008;29:780–9. doi:10.1016/j.biomaterials.2007.10.039.
29. Johansson JA, Halthur T, Herranen M, Soderberg L, Elofsson U, Hilborn J. Build-up of collagen and hyaluronic acid polyelectrolyte multilayers. Biomacromolecules 2005;6:1353–9. doi:10.1021/bm0493741.
30. Croll TI, O'Connor AJ, Stevens GW, Cooper-White JJ. A blank slate? Layer-by-layer deposition of hyaluronic acid and chitosan onto various surfaces. Biomacromolecules 2006;7:1610–22. doi:10.1021/bm060044l.
31. Richert L, Lavalle P, Payan E, Shu XZ, Prestwich GD, Stoltz JF, *et al*. Layer by layer buildup of polysaccharide films: Physical chemistry and cellular adhesion aspects. Langmuir 2004;20:448–58. doi:10.1021/la035415n.
32. Calvo P, RemunanLopez C, VilaJato JL, Alonso MJ. Novel hydrophilic chitosan-polyethylene oxide nanoparticles as protein carriers. J Appl Polym Sci. 1997;63:125–32. doi:10.1002/(SICI)1097-4628(19970103)63:1<125::AID-APP13>3.0.CO;2-4.
33. Janesand KA, Alonso MJ. Depolymerized chitosan nanoparticles for protein delivery: Preparation and characterization. J Appl Polym Sci. 2003;88:2769–76. doi:10.1002/app.12016.
34. Zhang H, Oh M, Allen C, Kumacheva E. Monodisperse chitosan nanoparticles for mucosal drug delivery. Biomacromolecules 2004;5:2461–8. doi:10.1021/bm0496211.
35. Kasaai MR, Arul J, Charlet C. Intrinsic viscosity-molecular weight relationship for chitosan. J Polym Sci B Polym Phys. 2000;38:2591–8. doi:10.1002/1099-0488(20001001)38:19<2591::AID-POLB110>3.0.CO;2-6.
36. Mosmann T. Rapid colorimetric assay for cellular growth and survival: application to proliferation and cytotoxicity assays. J Immunol Methods. 1983;65:55–63. doi:10.1016/0022-1759(83)90303-4.
37. Zange R, Li Y, Kissel T. Biocompatibility testing of ABA triblock copolymers consisting of poly(-lactic-co-glycolic acid) A blocks attached to a central poly(ethylene oxide) B block under *in vitro* conditions using different L929 mouse fibroblasts cell culture model. J Control Release. 1998;56:249–58. doi:10.1016/S0168-3659(98)00093-5.
38. He X, Ma J, Mercado AE, Xu W, Jabbari E. Cytotoxicity of paclitaxel in biodegradable self-assembled core-shell poly(lactide-co-glycolide ethylene oxide fumarate) nanoparticles. Pharm Res. 2008;25:1552-1562.
39. Fischer D, Li Y, Ahlemeyer B, Krieglstein J, Kissel T. *In vitro* cytotoxicity testing of polycations: influence of polymer structure on cell viability and hemolysis. Biomaterials 2003;24:1121–31. doi:10.1016/S0142-9612(02)00445-3.
40. Zhang Z, Huey Lee S, Feng SS. Folate-decorated poly(lactide-co-glycolide)-vitamin E TPGS nanoparticles for targeted drug delivery. Biomaterials 2007;28:1889–99. doi:10.1016/j.biomaterials.2006.12.018.
41. Alonso JL, Mascellaro S, Moreno Y, Ferrus MA, Hernandez J. Double-staining method for differentiation of morphological changes and membrane integrity of Campylobacter coli cells. Appl Environ Microbiol. 2002;68:5151–4. doi:10.1128/AEM.68.10.5151-5154.2002.
42. Valea FA, Haskill S, Moore DH, Fowler WC Jr. Immunohistochemical analysis of alpha 1-integrins in cervical cancer. Am J Obstet Gynecol. 1995;173:808–13. doi:10.1016/0002-9378(95)90345-3.
43. Green TR, Fisher J, Stone M, Wroblewski BM, Ingham E. Polyethylene particles of a [`]critical size' are necessary for the induction of cytokines by macrophages *in vitro*. Biomaterials 1998;19:2297–302. doi:10.1016/S0142-9612(98)00140-9.
44. Olivier V, Rivière C, Hindié M, Duval JL, Bomila-Koradjim G, Nagel MD. Uptake of polystyrene beads bearing functional groups by macrophages and fibroblasts. Colloids Surf B Biointerfaces. 2004;33:23–31. doi:10.1016/j.colsurfb.2003.08.008.
45. Zahr AS, Davis CA, Pishko MV. Macrophage uptake of core-shell nanoparticles surface modified with poly(ethylene glycol). Langmuir 2006;22:8178–85. doi:10.1021/la060951b.
46. Biological evaluation for medical devices-part 5: tests for cytotoxicity: *in vitro* methods. ISO 10993-5 (EN 30993-5), (1992).
47. Jepson MA. Advances in fluorescence imaging: opportunities for pharmaceutical science. Adv Drug Deliv Rev. 2005;57:1–4. doi:10.1016/j.addr.2004.08.001.
48. Huang M, Khor E, Lim LY. Uptake and cytotoxicity of chitosan molecules and nanoparticles: effects of molecular weight and degree of deacetylation. Pharm Res. 2004;21:344–53. doi:10.1023/B:PHAM.0000016249.52831.a5.
49. Maand ZS, Lim LY. Uptake of chitosan and associated insulin in Caco-2 cell monolayers: a comparison between chitosan molecules and chitosan nanoparticles. Pharm Res. 2003;20:1812–9. doi:10.1023/B:PHAM.0000003379.76417.3e.
50. Harush-Frenkel O, Debotton N, Benita S, Altschuler Y. Targeting of nanoparticles to the clathrin-mediated endocytic pathway. Biochem Biophys Res Commun. 2007;353:26–32. doi:10.1016/j.bbrc.2006.11.135.
51. Ruponen M, Honkakoski P, Tammi M, Urtti A. Cell-surface glycosaminoglycans inhibit cation-mediated gene transfer. J Gene Med. 2004;6:405–14. doi:10.1002/jgm.522.
52. Lemarchand C, Gref R, Passirani C, Garcion E, Petri B, Muller R, *et al*. Influence of polysaccharide coating on the interactions of nanoparticles with biological systems. Biomaterials 2006;27:108–18. doi:10.1016/j.biomaterials.2005.04.041.
53. Peerand D, Margalit R. Loading mitomycin C inside long circulating hyaluronan targeted nano-liposomes increases its antitumor activity in three mice tumor models. Int J Cancer. 2004;108:780–9. doi:10.1002/ijc.11615.
54. Lemarchand C, Gref R, Couvreur P. Polysaccharide-decorated nanoparticles. Eur J Pharm Biopharm. 2004;58:327–41. doi:10.1016/j.ejpb.2004.02.016.